

Supporting Information

CoNCNTs anchoring Ru/RuO₂ heterojunction nanostructures as an electrocatalyst for highly effective water splitting

Zhenjiang Lu, Qiaoling Zhao, Jing Xie, Jindou Hu, *Bai Sun**, Yali Cao*

State Key Laboratory of Chemistry and Utilization of Carbon Based Energy Resources; Key Laboratory of Advanced Functional Materials, Autonomous Region; Institute of Applied Chemistry, College of Chemistry, Xinjiang University, Urumqi 830017, PR China.

E-mails: caoyali523@163.com (Y.C.)

2.1. Chemicals

Cobalt nitrate hexahydrate (Co(NO₃)₂·6H₂O, 99 wt%), melamine (C₃H₆N₆, 98%), zinc nitrate hexahydrate (Zn(NO₃)₂·6H₂O, 99 wt%), Ruthenium trichloride hydrate (RuCl₃·3H₂O), isopropyl alcohol (C₃H₈O), ethanol (C₂H₆O), Nafion solution (5 wt%), Pt/C (20 wt%), commercial carbon nanotubes, and commercial RuO₂ were purchased from Aladdin Ltd. All chemicals were used as received without further purification. In all experiments, deionized water was used from a millipore.

2.2. Materials characterization

The phase structure was identified using powder X-ray diffraction (XRD) on a Rigaku Smart Lab SE diffractometer. The morphology of samples was investigated by field emission scanning electron microscope (FESEM, Hitachi S-4800H), transmission electron microscopy (TEM, JEM-2100F), high resolution transmission electron microscope (HRTEM, JEOL JEM-2010F), and elemental mapping were obtained from JEOL JEM-2100F microscope. The precise content of each component in the composite were determined by an inductively coupled plasma-optical emission spectrometer (ICP-OES, Optima 8000). X-ray photoelectron spectroscopy (XPS) was measured to study the element composition and electron states using a ThermoFisher ESCALAB 250 xi. Raman spectra were collected on a Smart System HR Evolution (Horiba JobinYvon,

France).

2.3 Electrochemical measurement

The electrochemical test was carried out on an electrochemical workstation (CHI760E, Shanghai Chenhua, China) utilizing the three-electrode system. The electrocatalytic HER performance of the as-prepared catalysts was investigated in a typical three-electrode system by linear sweep voltammetry (LSV) in N₂-saturated 1.0 M KOH at a scan rate of 10 mV s⁻¹ after iR correction. The working electrode was the L-shaped glassy carbon electrode with a diameter of 4 mm. The Hg/HgO electrode and platinum wire were used as reference and counter electrodes, respectively. In generally, 2.5 mg catalyst was dispersed in a mixture of 340 μL isopropyl alcohol, 150 μL deionized water and 10 μL 5 wt% Nafion. Subsequently, after ultrasonic treatment for 60 min, the catalyst suspension of 10 μL was uniformly dropped onto the surface of the glassy carbon electrode and dried at room temperature. Linear sweep voltammetry measurements were taken at scan rates of 10 mV s⁻¹. In this work, all the potentials were referenced to a reversible hydrogen electrode (RHE) computed by the following equation: $E_{RHE} = E_{Hg/HgO} + 0.059 * pH + E^0_{Hg/HgO}$. The overpotential (η) in the case of OER was calculated according to the literature reported by the following equation: $\eta (V) = E_{RHE} - 1.23V$. Tafel slopes were derived from polarization curves using the equation: $\eta = a + b \log |j|$, where η and j are overpotentials and current density measured using the geometric area of the electrode; the Tafel slopes were represented by b . The IR-correction of the measured potentials from the LSV profiles for both the OER and HER was executed using Equation:

$$E_{IR} = E_{(V \text{ vs } RHE)} - IRs \quad (1)$$

The electrochemically active surface area (ECSA) of the electrocatalysts was calculated using Equation :

$$ECSA = \frac{C_{dl}}{C_s} \quad (2)$$

where C_{dl} is the electric double-layer capacitance calculated from the non-Faradaic region, and C_s is the specific capacitance of the cyclic voltammogram (CV) was

measured at scan rates of 20, 40, 60, 80, 100, 120, 140, 160, 180, and 200 mV s⁻¹.

2.4 Calculation methods

2.4.1 The calculation for Turnover frequency (TOF)

The TOF value was calculated based on estimated numbers of active sites^[1]

$$TOF = \frac{\text{Total oxygen turnovers}}{\text{The number of active sites (N)}} \quad (3)$$

The values of the total hydrogen (or oxygen) turnovers were calculated from the current density obtained in the OER (or HER) polarization:

HER

$$\begin{aligned} H_2 & : \\ & = j_{HER} * \frac{mA}{cm^2} * \frac{1 C s^{-1}}{1000 mA} * \frac{1 mol e s^{-1}}{96435.3 C} * \frac{1 mol O_2}{2 mol e^{-1}} * \frac{6.02 * 10^{23} mol}{1 mol H_2} \\ & = 3.12 * 10^{15} * \frac{H_2 s^{-1}}{cm^2} * per \frac{mA}{cm^2} \end{aligned} \quad (4)$$

OER

$$\begin{aligned} O_2 & : \\ & = j_{OER} * \frac{mA}{cm^2} * \frac{1 C s^{-1}}{1000 mA} * \frac{1 mol e s^{-1}}{96435.3 C} * \frac{1 mol O_2}{4 mol e^{-1}} * \frac{6.02 * 10^{23} mol}{1 mol O_2} \\ & = 1.56 * 10^{15} * \frac{O_2 s^{-1}}{cm^2} * per \frac{mA}{cm^2} \end{aligned} \quad (5)$$

Thus,

$$TOF_{HER} = (3.12 \times 10^{15} H_2 s^{-1} cm^{-2} per(mA cm^{-2}) \times |j|) / N \quad (6)$$

$$TOF_{OER} = (1.56 \times 10^{15} O_2 s^{-1} cm^{-2} per(mA cm^{-2}) \times |j|) / N \quad (7)$$

The catalyst load on the glassy carbon electrode (the diameter of the glassy carbon

electrode is 4 mm) is $0.4 \text{ mg} \cdot \text{cm}^{-2}$, so the load of Ru element on the glassy carbon electrode is calculated as follows:

$$m_{Ru} = 0.4 \text{ mg cm}^{-2} \times \text{wt\% (Ru)} \quad (8)$$

We assume that all RuO_2 atoms in the catalysts are active for OER, and Ru atoms are active for HER. The numbers of RuO_2 and Ru atoms number in $\text{RuO}_2/\text{Ru@CoNCNTs-30}$ catalyst were calculated from the RuO_2 and Ru molar mass loading on the CoNCNTs. The Ru content of catalyst determined by ICP-MS measurement was 1.1 wt.%, and the mass ratios of $\text{Ru}^{4+}/(\text{Ru}^{4+} + \text{Ru}^0)$ for Ru@CoNCNTs-30 is calculated to be 58.2% by XPS. Thus, the content of RuO_2 in $\text{RuO}_2/\text{Ru@CoNCNTs-30}$ is 0.64%, and the Ru is 0.36%.

The number of active sites (N) is further calculated by the following equation:

$$\text{Surface active site (N)} = (0.4 \times 10^{-3} \times \text{wt\%} \times \text{at\%} \times 6.023 \times 10^{23}) / M \text{ mol}^{-1} \quad (9)$$

$$\begin{aligned} N_{Ru} &= \frac{0.36}{100} * \frac{0.40 \text{ mg}}{\text{cm}^2} * \frac{1}{101.1 \text{ mg mol}} * \frac{6.02 * 10^{20} \text{ sites}}{\text{mol}} \\ &= 8.57 * 10^{15} \text{ sites cm}^{-2} \end{aligned} \quad (10)$$

$$\begin{aligned} N_{RuO_2} &= \frac{0.64}{100} * \frac{0.40 \text{ mg}}{\text{cm}^2} * \frac{1}{133.1 \text{ mg mol}} * \frac{6.02 * 10^{20} \text{ sites}}{\text{mol}} \\ &= 1.16 * 10^{16} \text{ sites cm}^{-2} \end{aligned} \quad (11)$$

2.4.2 The calculation for mass activity

Mass activity ($\text{A g}^{-1} \text{ metal}$) was obtained by normalizing current density (mA cm^{-2}) by mass loading (0.022 mg cm^{-2}) at a certain overpotential according to the equation:

$$J_{\text{mass activity}} = \frac{J_{\text{HER(or OER)}} * \frac{\text{mA}}{\text{cm}^2}}{m_{Ru} * \text{g}} \quad (12)$$

2.4.3 Theoretical calculations

All Density Functional Theory (DFT) calculations were performed on the Vienna Ab initio Simulation Package (VASP) by using the PBE exchange-correlation function. The interaction between valence electrons and the ionic core was described by the PAW pseudo-potential. The geometry structures were optimized with the cutoff energy of 400 eV. All atoms are allowed to relax until the magnitude of all residual forces was less than 0.02 eV. Ionic relaxations were carried out under conventional energy (10 - 5 eV). The Monkhorst-Pack k-point mesh of $3 \times 3 \times 1$ was used to calculate the density of states and Gibbs free energy. For the calculation of transition states, CI-NEB method and DIMER method were used.

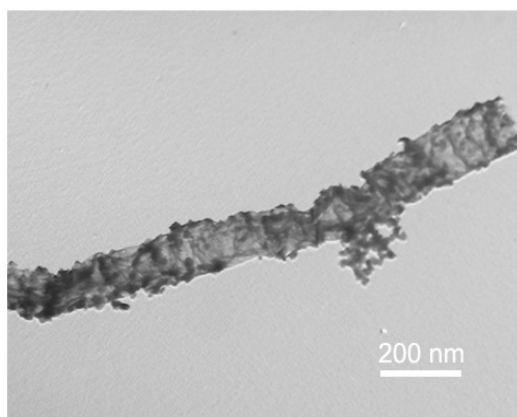


Figure S1. The TEM image of RuO₂/Ru@CoCNTs-30.

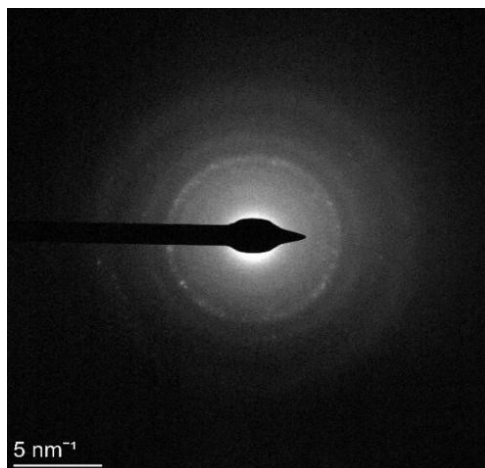


Figure S2. The selected-area electron diffraction pattern of RuO₂/Ru@CoNCNTs-30.

Table S1. Element contents (wt%) of different samples characterized by ICP-OES.

Samples	Ru content (Wt%)	Co content (Wt%)
RuO ₂ /Ru@CoNCNTs-20	0.8	14.6
RuO ₂ /Ru@CoNCNTs-30	1.1	13.7
RuO ₂ /Ru@CoNCNTs-40	1.3	13.3
RuO ₂ /Ru@CoNCNTs-30-4h	1.5	12.9
Commercial RuO ₂	20	/

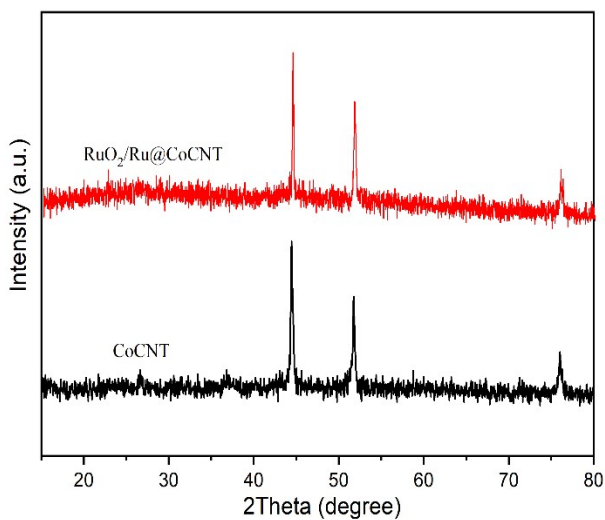


Figure S3. The XRD patterns of RuO₂/Ru@CoCNTs and CoCNTs.

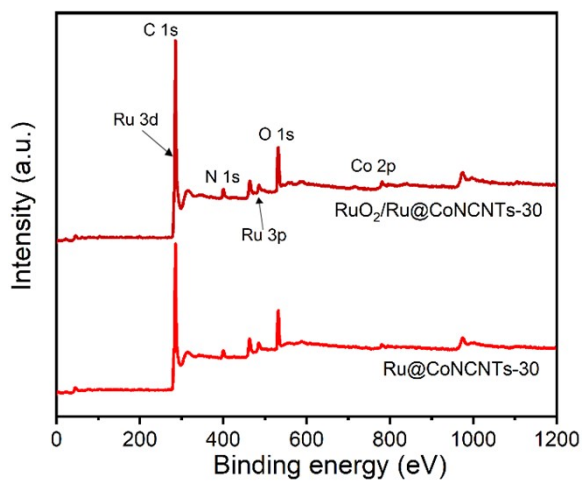


Figure S4. XPS survey spectra.

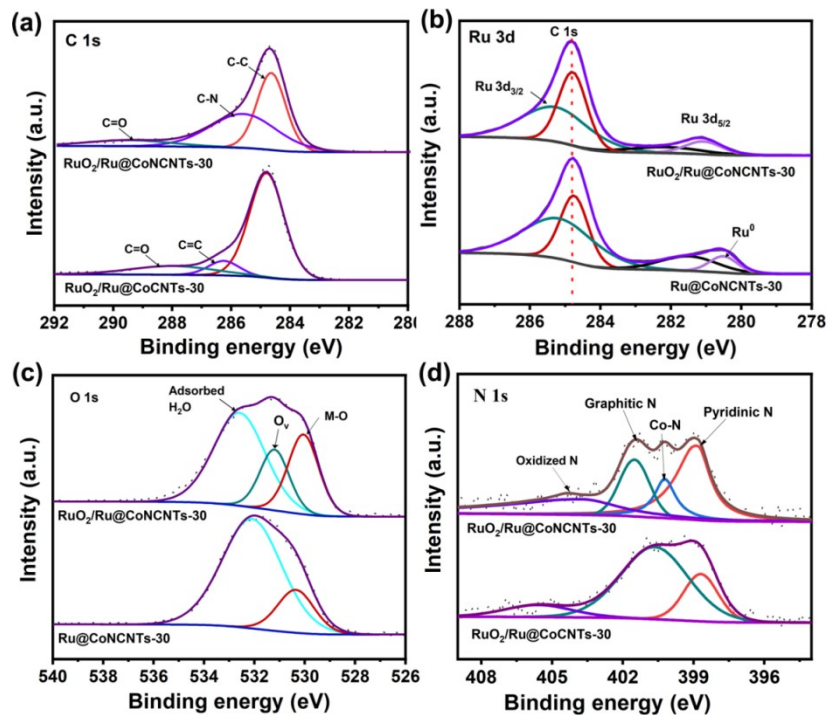


Figure S5. High-resolution XPS spectra of C 1s, Ru 3d, O 1s and N 1s of Ru/RuO₂@Co@NCNTs-30 and Ru/Co@NCNTs-30.

Table S2. Curvefit parameters for Ru R-edge EXAFS of RuO₂/Ru@CoNCNTs.

Sample	element	path	CN	R(Å)	ΔE_0 (eV)	σ^2 (Å ²)	R-factor
RuO ₂ /Ru	Ru	Ru-Ru	4.146	2.680	-7.08	0.00654	0.009
	Ru, O	Ru-O	5.458	1.966	-7.08	0.00826	0.009

CN: Coordination numbers; R: bond distance; ΔE_0 : the inner potential correction; σ^2 : Debye-Wallerfactors; R-factor: goodness of fit.

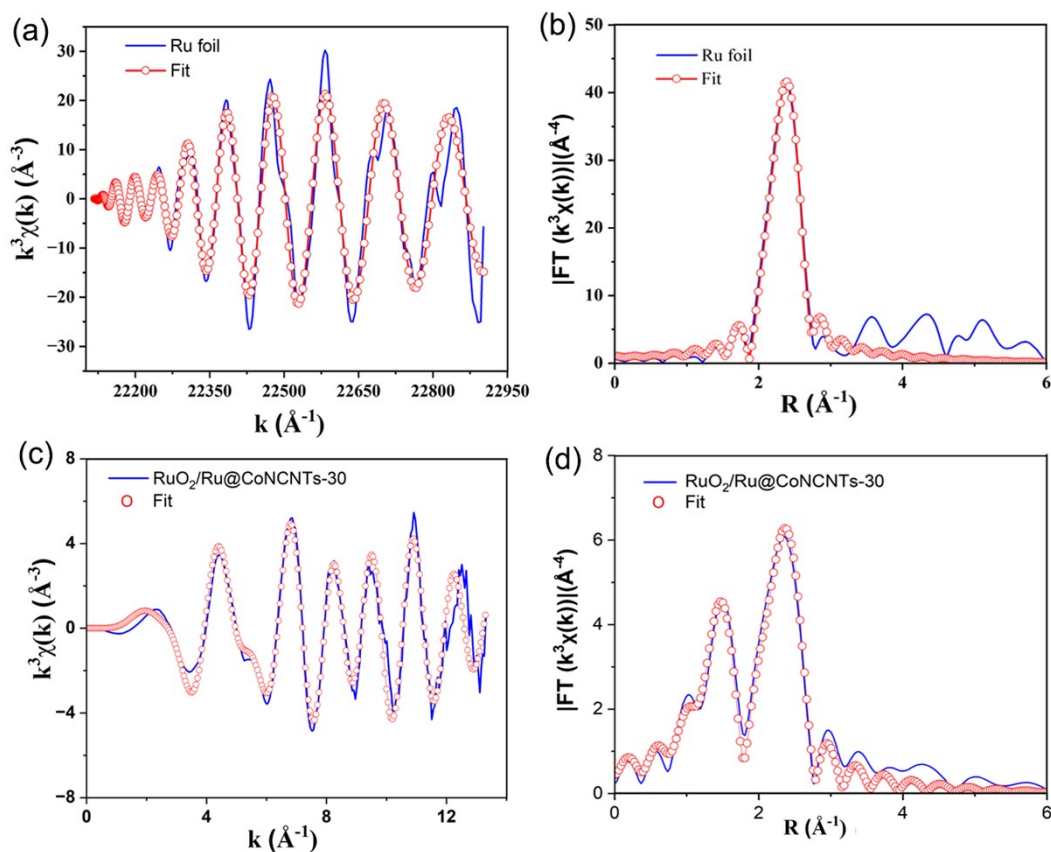


Figure S6. EXAFS fit of Ru.

Table S3. Curvefit parameters for Co R-edge EXAFS of RuO₂/Ru@CoNCNTs.

Sample	element	path	CN	R(Å)	ΔE_0 (eV)	σ^2 (Å ²)	R-factor
CoNCNTs	Co	Co-Co	3.939	2.856	-8.93	0.00486	0.00306
	Co	Co-Co	7.026	3.366	-8.93	0.00769	0.0188
	Co, O	Co-O	4.580	1.925	-8.93	0.00415	0.00714

CN: Coordination numbers; R: bond distance; ΔE_0 : the inner potential correction; σ^2 : Debye-Waller factors; R-factor: goodness of fit.

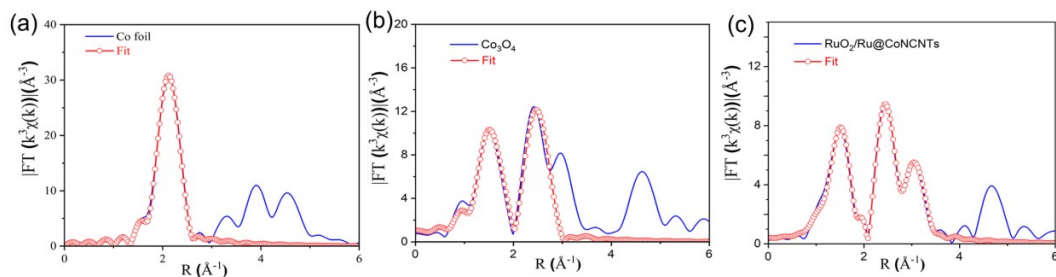


Figure S7. EXAFS fit of Co.

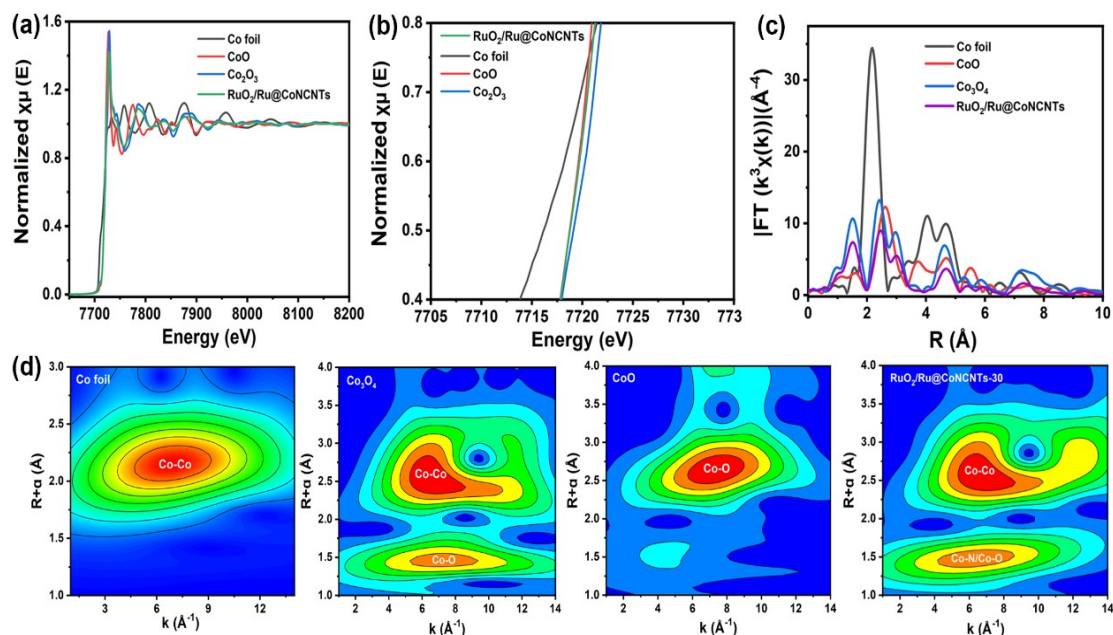


Figure S8 (a-b) K-edge XANES spectra. (c) EXAFS spectra in R space. (d) WT-EXAFS spectra of Co.

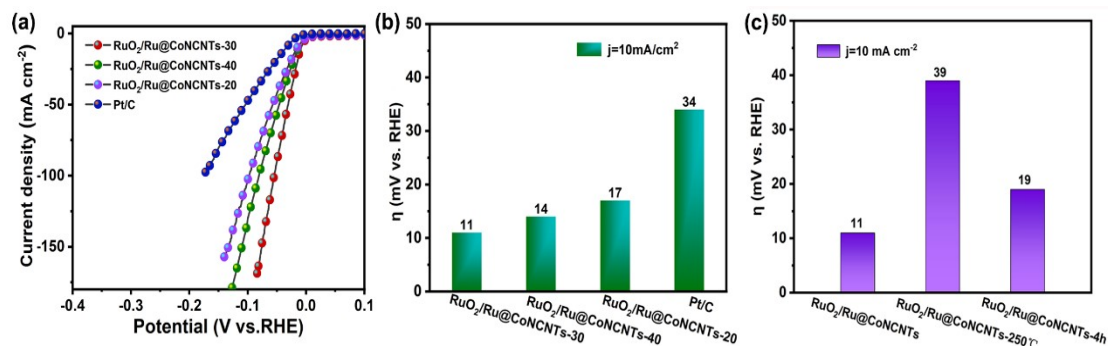


Figure S9. (a) LSV curves for HER of different samples. (b-c) Overpotentials at 10 mA cm⁻².

Table S4. Comparison of Ru/RuO₂@Co@NCNTs-30 with many recently reported precious metals (Pt, Ru and Ir) based HER catalyts.

Catalyst	HER		Ref.
	η_{10} , mV	Tafel slope	
Ru/RuO ₂ @Co@NCNTs-30	11	21	This work
Ru-FeNi@NLC	36	36	Angew. Chem. Int. Ed., 2023, 62, e202306333.
CoNiRu-NT	22	56	Adv. Mater., 2022, 2107488.
RuNi@C	31	30	J. Mater. Chem. A, 2020, 8, 9049-9057.
RuNi alloy-CFC	43	37	Nanoscale 2021, 13, 13042-13047.

RuNi@SC-CNT	55	96	Chem. Eng. J., 2021, 417, 129319.
NiRu@Fe/C@CNT	32	54	Chem. Eng. J., 2021, 424, 130416.
RuCoO _x	37	53	J. Mater. Chem. A, 2018, 6, 18948.
PtCo/C NW	32	33.9	ACS Appl. Mater. Interfaces, 2022, 14, 25246.
Ru/RuO ₂	17	53	Energy Environ. Sci., 2021,14, 5433.
Ir@Rhene/C	17	15	Adv. Sci., 2023,10, 2302358.
Pt@Cu	35	61	Adv. Funct. Mater. 2021, 31, 2105579.
Ru SAs-MoO _{3-x} /NF	36	41	Adv. Sci., 2023, 10, 2300342.
Ru/RuO ₂ nanosheets	20	23	Sci. Bull., 2022, 67, 2103.
Au@Pt _{1.5} Co _{0.08}	14	29	J. Energy Chem., 2022, 69, 44-53.
Pt-Ni ₄ Mo/CNT	18.6	37.4	J. Mater. Chem. A, 2022, 10, 15395-15401.
Ru ₂ Co ₁ BO-350	14	25	Nano Lett. 2023, 23, 3, 1052-1060.
Pt/NP-CNT	25	28	J. Mater. Chem. A, 2022, 10, 16403-16408.
Ru-CuO-SA	13	28	Nano Energy, 2023, 111, 108403.
Ru/RuO ₂ Aerogels	34	29	Small, 2023,19, 2206844.
d-Pt-Ni NWs	15	29	ACS Materials Lett. 2021, 3, 12, 1738-1745.
Cu-doped Ru/RuSe ₂ NSs	23	59	Adv. Mater., 2023,35, 2300980.
Cu-Ru/Ti	23	34	J. Mater. Chem. A, 2020,8, 10787-10795.
Ru/Co-N-C	23	23	Adv. Mater., 2022,34, 2110103.
Ru@MoO(S) ₃	30	29	Nano Energy, 2022, 100, 107445.
RuO ₂ NB/C	45	31	Chem. Eng. J., 2023, 468,143761
RuCo	25	45	Adv. Energy Mater., 2023,13, 2301119
CoVru LDH	28	25.4	Chem. Eng. J., 2023, 452,139151

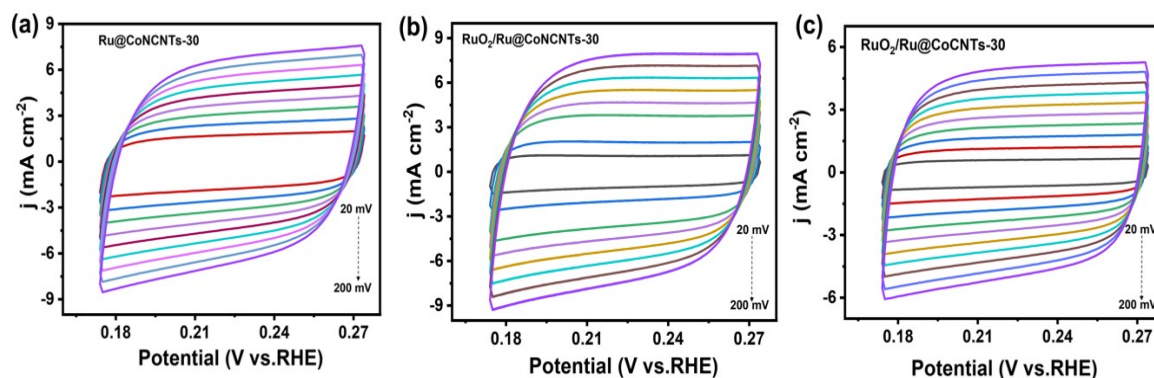


Figure S10. The HER CV curves of different samples with scan rates from 20 mV s⁻¹ to 200 mV s⁻¹ in 1.0 M KOH.

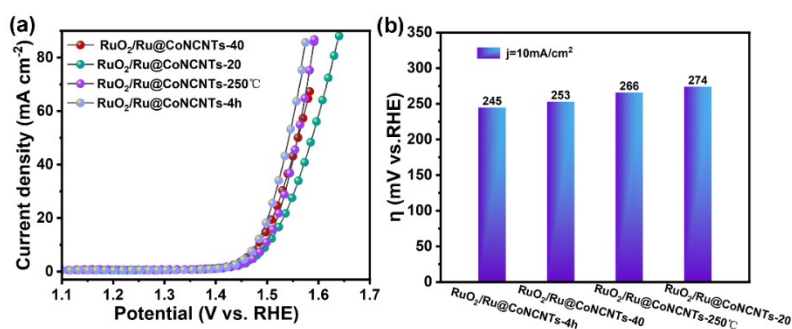


Figure S11. (a) LSV curves, and (b) Overpotentials at 10 mA cm⁻² for OER of different samples.

Table S5. Comparison of Ru/RuO₂@Co@NCNTs-30 with many recently reported precious metals (Pt, Ru and Ir) based water splitting catalysts.

Catalyst	HER	Tafel	OER	Tafel	Cell voltage	Ref.
	η ₁₀ , mV	slope	η ₁₀ , mV	slope	(V) 10 mA/cm ²	
Ru/RuO₂@Co@NCNTs-30	11	21	234	69	1.46	This work
Ru-FeNi@NLC	36	36	198	72	1.47	Angew. Chem. Int. Ed., 2023, 62, e202306333.
CoNiRu-NT	22	56	255	67	1.47	Adv. Mater., 2022, 2107488.
RuNi@C	31	30	278	46	1.51	J. Mater. Chem. A, 2020, 8, 9049.
NiRu@Fe/C@CNT	32	54	246	46	1.51	Chem. Eng. J. 2021, 424, 130416.
RuCoO _x	37	53	275	54	1.54	J. Mater. Chem. A, 2018, 6, 18948.
Ru SAs-MoO _{3-x} /NF	36	41	206	55	1.49	Adv. Sci., 2023, 10, 2300342.
Ru ₂ Co ₁ BO-350	14	25	219	58	1.47	Nano Lett. 2023, 23, 3, 1052-1060.
Ru/RuO ₂ Aerogels	34	29	189	68	1.47	Small, 2023, 19, 2206844.
Ru/Co-N-C	23	23	247	66	1.47	Adv. Mater., 2022, 34, 2110103.
Ru@MoO(S) ₃	30	29	265	47	1.53	Nano Energy, 2022, 100, 107445.
RuO ₂ NB/C	45	31	273	69	---	Chem. Eng. J., 2023, 468, 143761.
RuCo	25	45	245		1.49	Adv. Energy Mater., 2023, 13, 2301119.
CoVru LDH	28	25.4	263	75	1.53	Chem. Eng. J., 2023, 452,139151

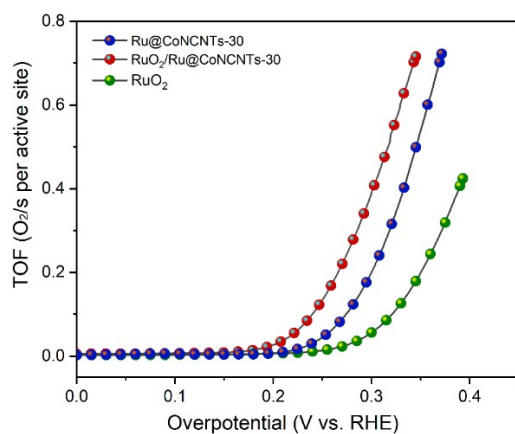


Figure S12. The TOF values of catalyst for HER in 1 M KOH.

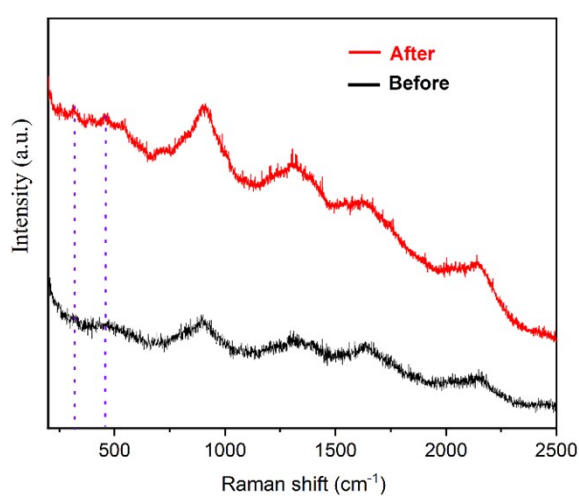


Figure S13. Raman spectra of RuO₂/Ru@CoNCNTs-30 before and after OER test.

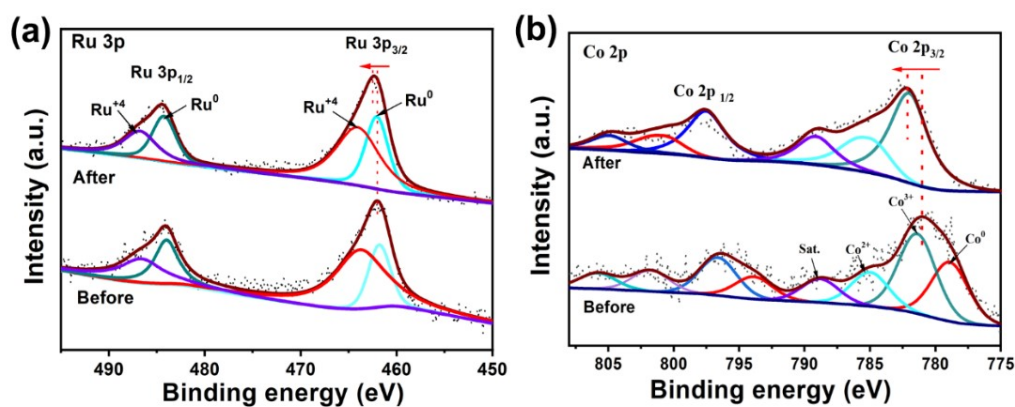


Figure S14. High-resolution XPS spectra of (a) Ru 3p, and (b) Co 2p of RuO₂/Ru@CoNCNTs-30 after the OER test.

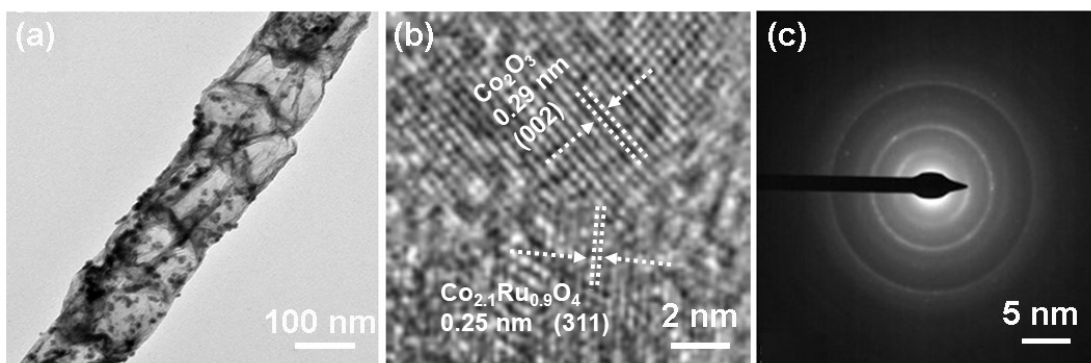


Figure S15. (a-b) HRTEM, (c) SAED of RuO₂/Ru@CoNCNTs-30.

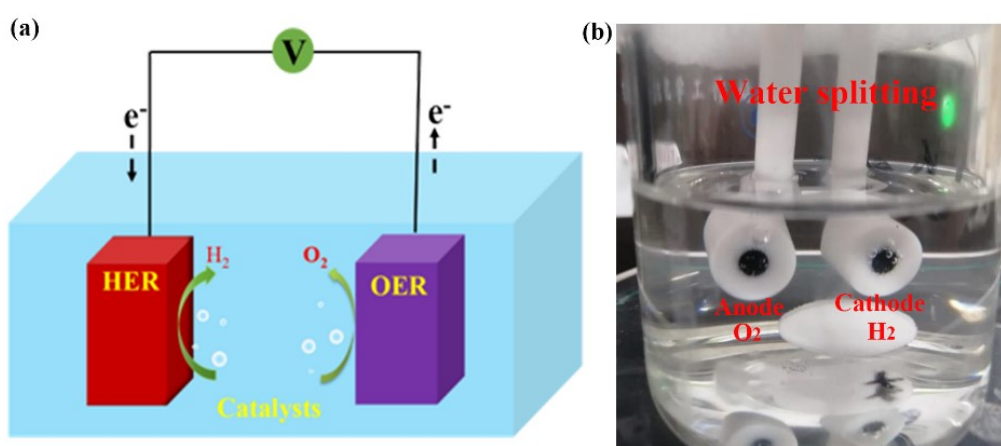


Figure S16. (a) The schematic diagram of electrolytic water equipment, (b) Digital photograph of two-electrode setup for RuO₂/Ru@CoNCNTs-30//RuO₂/Ru@CoNCNTs-30.

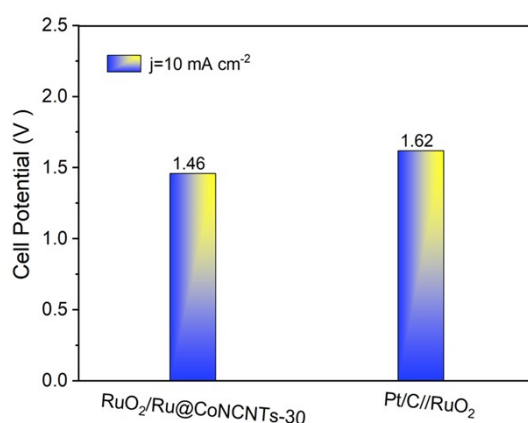


Figure S17. The voltage of cell at 10 mA cm⁻².

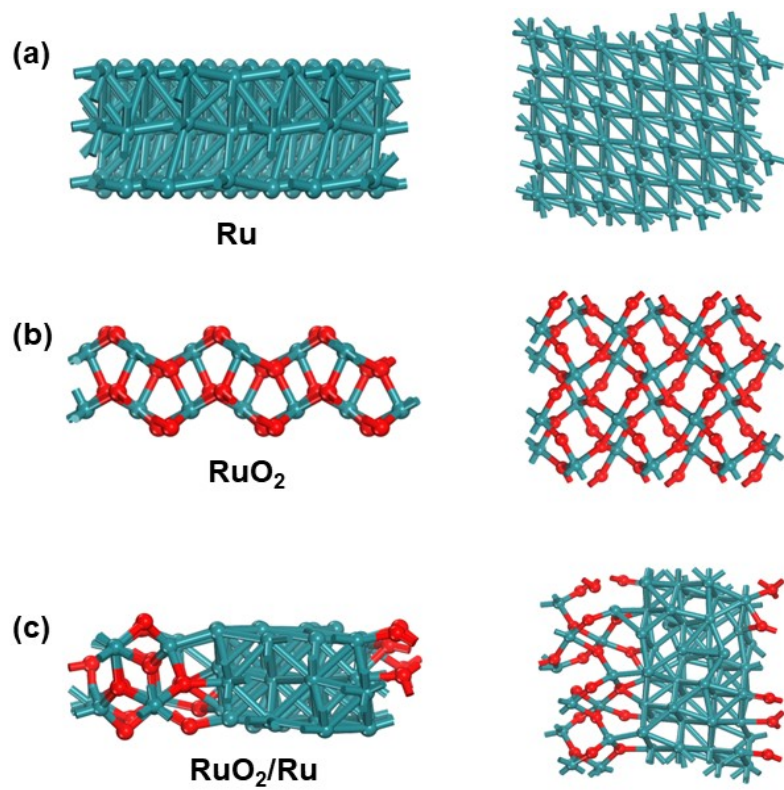


Figure S18. Theoretical models of (a) Ru, (b) RuO₂, and (c) RuO₂/Ru systems.

[1] C. Rong, X. Shen, Y. Wang, L. Thomsen, T. Zhao, Y. Li, X. Lu, R. Amal, C. Zhao, *Adv. Mater.*, **2022**, 34.